632 | https://doi.org/10.3311/PPci.44549
Creative Commons Attribution

Periodica Polytechnica Civil Engineering, 70(2), pp. 632–642, 2026

SGS-based Reliability Assessment of Driven Piles at Solar Farm Sites

Bence Kató[1], András Mahler[2*]

[1] College of Civil and Transportation Engineering, Shenzhen University, 3688 Nanhai Avenue, Nanshan District, 518060 Shenzhen, Guangdong Province, China
[2] Department of Engineering Geology and Geotechnics, Faculty of Civil Engineering, Budapest University of Technology and Economics, Műegyetem rkp. 3., H-1111 Budapest, Hungary
[*] Corresponding author, e-mail: mahler.andras@emk.bme.hu

Received: 04 May 2026, Accepted: 01 June 2026, Published online: 12 June 2026

Abstract

Utility-scale solar farms require reliable design of tens of thousands of driven steel pile foundations, where wind-induced uplift governs. Spatial variability of the shallow subsurface and limited cone penetration test (CPT) coverage mean pile reliability depends on distance from the nearest test – an uncertainty Eurocode 7 does not capture. This paper proposes a probabilistic methodology combining sequential Gaussian simulation (SGS) of CPT data with three capacity methods (LCPC, AFNOR NF P 94-262 and ICP-05) and FOSM/FORM reliability analysis to quantify uplift reliability along linear Chains connecting adjacent CPT locations. The methodology is applied to a solar farm in Pleistocene sandy deposits with 70 CPTs. Two Chains are analyzed: a 309 m Chain through five CPTs in a uniform zone and a 302 m Chain through four CPTs in a variable zone. Pile reliability is governed by two independent contributions. The first is conditioning geometry: the COV of uplift resistance is smallest at CPT locations and grows with distance, forming a wave-like profile with minima of 1.4–2.7% at CPTs and maxima of 3.2–6.1% at midpoints. The second is geological variability: differences in soil strength shift the mean resistance and dominate the reliability index wherever the deposit is non-uniform. Along Chain 1, the FORM reliability index β varies only moderately, driven almost entirely by conditioning geometry. Along Chain 2, β spans a range over three times wider, reflecting dominant geological heterogeneity. The Chain-based framework provides a site-specific basis for separating these contributions, for optimizing CPT spacing and delineating geological zones.

Keywords

driven steel piles, uplift resistance, soil spatial variability, sequential Gaussian simulation, reliability analysis, cone penetration test

1 Introduction

The global transition toward renewable energy has driven a remarkable expansion of utility-scale photovoltaic (PV) solar panel installations. A typical solar farm of 50–100 MW capacity requires between 20,000 and 100,000 individual pile foundations to support the panel mounting structures [1]. These foundations are predominantly prefabricated steel sections, most commonly H-piles (e.g., HEA profiles) or channel sections (e.g., SIGMA profiles), driven into the ground to depths of 2–6 m [2, 3]. Unlike conventional building or bridge foundations, solar farm piles are designed primarily to resist wind-induced uplift and lateral forces rather than large compressive loads, making tensile (pull-out) capacity their governing design criterion [4]. The geotechnical design of these foundations must ensure adequate safety against uplift failure over the 25–35 year design life of the installation, typically across sites that can span multiple square kilometers. At this scale, the spatial variability of subsurface conditions becomes a significant concern: soil properties can change markedly across pile locations, yet a single, representative ground model is commonly used for the entire site or for large sub-zones within it [5]. The mismatch between the assumed homogeneity and the actual heterogeneity of the ground introduces design uncertainty that is not fully captured by conventional safety factors.

In current European practice, the design of pile foundations follows the partial factor method prescribed by EN 1997-1 (Eurocode 7) [6]. When the pile resistance is derived from ground test results (e.g., CPT data), the standard requires the application of correlation factors (ξ) to

Cite this article as: Kató, B., Mahler, A. "SGS-based Reliability Assessment of Driven Piles at Solar Farm Sites", Periodica Polytechnica Civil Engineering, 70(2), pp. 632–642, 2026. https://doi.org/10.3311/PPci.44549

account for ground variability that depend on the number of tests available. Larger number of available tests lead to smaller correlation factors, reflecting increased confidence in the representativeness of the design ground model [6, 7]. However, the correlation factors are often applied globally and do not differentiate between locations where the spatial variability is high or low, nor do they account for the distance between the test locations and the location of individual piles.

The objective of this paper is to investigate how the spatial arrangement of cone penetration test (CPT) soundings affects the uncertainty in the predicted uplift resistance of solar panel foundations and the resulting reliability index. A probabilistic framework based on the sequential Gaussian simulation (SGS) of CPT data is proposed, complemented by a Chain-based sampling strategy that places virtual CPT points at uniform spacing along straight lines connecting real CPT locations. This sampling strategy is shown to be essential for separating the geometric effect of the investigation distance from the underlying geological variability of the soil. The methodology is demonstrated through a case study involving approximately 70 CPT soundings at a planned solar farm site in Pleistocene sandy deposits.

2 Recent practice

Driven steel piles are the most widely adopted foundation type for utility-scale solar farms because their installation is both fast and economical. A relatively shallow embedment of steel piles is sufficient to mobilize the required pull-out resistance, no concrete curing is involved, and drive rates of 200–500 piles per day per driving rig are common, providing significant schedule advantages over cast-in-place alternatives [4, 8]. The loading regime of solar panel foundations, however, differs fundamentally from that of buildings. Solar panel arrays are lightweight structures with small self-weight and large surfaces. Therefore, gravity loads are insignificant compared with wind loads acting on the panel surface. Therefore, the dominant design loads are wind-induced uplift forces on the windward pile row and combined compression-moment loading on the leeward piles [2, 9]. Considering design wind speeds according to regional standards (e.g., EN 1991-1-4 standard [9] in Europe), the resulting characteristic uplift force on an individual pile is typically in the range of 10–50 kN, depending on panel geometry, tilt angle and exposure to the major wind direction [2, 4]. Because the piles are slender with a shallow embedment depth, the uplift resistance is mobilized almost entirely through shaft friction along the soil-pile interface, with negligible contribution from the pile toe [10]. Reliable design therefore hinges on an accurate prediction of the unit shaft friction in tension along the upper few meters of the soil profile, where the variability of natural deposits is most pronounced.

In European practice, the design of these piles is governed by EN 1997-1 (Eurocode 7) [6], which prescribes limit state verification with partial factors applied to actions and resistances. The standard permits to derive the characteristic tensile resistance of steel piles from static load tests, dynamic load tests or, from CPT-based empirical correlations [7]. In solar farm projects, where individual pile testing across an entire site is economically impractical, the latter is most commonly adopted. After the pile characteristic tensile resistance is derived from CPT results, Eurocode 7 [6] requires the application of correlation factors, ξ_3 or ξ_4, that depend solely on the number of test profiles available, and decreases the characteristic value to account for statistical uncertainty and limited sampling. The design tensile resistance, $R_{t,d}$, is then obtained by dividing the characteristic resistance by the partial resistance factor $\gamma_{s,t}$ (typically 1.25–1.60 depending on the National Annex and Design Approach adopted) [6, 11]. Several well-established direct CPT-based methods are available to estimate the ultimate shaft friction of steel piles. The most common ones are the LCPC method of Bustamante and Gianeselli [12], the NF P 94-262 standard [13] by the AFNOR, and the ICP-05 method [10], that all require the classification of the soil profile in order to select appropriate coefficients during the calculations. The Robertson [14] soil behavior type (SBT) classification is widely used for this purpose. Despite the maturity of these procedures, the EC7 correlation factors (ξ) are calibrated for generic conditions and do not take into account either the site-specific spatial variability of the soil or the distance between the CPT location and the pile [15], which are the central limitations that motivate the present work.

Research specifically addressing the geotechnical design of solar farm pile foundations has emerged primarily in the last decade. Kelly et al. [2] presented one of the most comprehensive contributions to date, combining Monte Carlo simulations with unsaturated soil mechanics to assess pile displacements in expansive clays. Their analysis showed that the largest movements are associated with extreme wetting or drying events and that the predicted displacements are sensitive to the probability distributions assumed for the governing input parameters (e.g., soil and load parameters). This sensitivity to probability distributions has been further highlighted

in geotechnical limit state problems by Chemali and Tiliouine [16], who showed that lognormally distributed design variables yield substantially different reliability indices than normally distributed ones. In a closely related context, the offshore wind energy sector has produced parallel work on tensile-loaded driven piles. Cai et al. [17, 18] developed a CPT-based framework for tension-loaded open-ended piles in spatially heterogeneous sandy soils, in which the design resistance profile along the pile was optimized to achieve a specified target reliability. They demonstrated that the appropriate statistical approach for constructing this profile depends on both the spatial proximity of the nearest CPTs to the pile and the spatial variability characteristics of the cone tip resistance, including its scale of fluctuation and coefficient of variation. Their work, however, employed synthetic random fields with prescribed statistical properties rather than site-specific geostatistical simulations conditioned on real CPT data, which limits its direct applicability to practical engineering projects. The broader question of soil property uncertainty in geotechnical design has been treated extensively by Phoon and Kulhawy [19, 20], who identified inherent spatial variability, measurement error, and transformation uncertainty as its three principal sources. These have direct implications for pile design: the vertical averaging of soil properties along the pile shaft artificially reduces parameter variance [19, 20], while disregarding the horizontal variability of soils away from the CPT location, misses how representative the selected CPT profile is for various pile locations. Although the partial factor method, as prescribed by EN 1990 standard [21], aims to achieve a target reliability index of $\beta \approx 3.3–3.8$ for 50-year reference periods (corresponding to annual failure probabilities of about 10^{-4} to 10^{-5}), the actual reliability achieved at any specific pile location depends on the site-specific spatial variability of the soil, which routine design does not assess explicitly [15]. For solar farm sites in particular, where the number of foundations is very large and the consequences of an individual pile failure are comparatively modest, there is a strong case for calibrating the design against a site-specific target reliability rather than relying on uniform, code-based correlation factors [2], to optimize design and economy. Geostatistical simulations provide a natural framework for such probabilistic assessments. Sequential Gaussian simulation (SGS) [22, 23] is among the most widely applied techniques for generating conditional realizations of spatially correlated random fields. In SGS the variable of interest is first transformed to a standard normal distribution and then simulated sequentially on a grid by drawing the value of each node from the local conditional distribution obtained from simple kriging [24, 25]. Unlike deterministic interpolation methods (e.g., kriging), which return a smoothed best estimate, SGS generates an ensemble of realizations that each honor the observed data at measurement locations, reproduce the histogram and the spatial correlation structure of the original field, and exhibit the same level of spatial variability as the real data [24, 25]. The SGS ensemble can therefore be interrogated directly to obtain a quantitative measure of the predictive uncertainty at any unmeasured point. To the authors' knowledge, however, the combination of site-specific SGS applied to dense CPT data for the explicit probabilistic assessment of driven pile uplift resistance at solar farm sites, with particular attention to the effect of the investigation distance, has not been reported in the literature, and addressing this gap is the central aim of the present study.

3 Methods

The study site is in a region characterized by Pleistocene alluvial and fluvial deposits. The subsurface conditions within the pile embedment zone (upper 3–5 m) consist predominantly of medium-dense to dense sandy soils, according to the Robertson soil behavior type classification (SBT zones 5–6, $I_c \approx 1.3–2.0$ over most of the pile depth, with locally higher values where weaker silty or clayey lenses occur). The groundwater table is located at approximately 5 m below the prepared ground level, i.e., the pile tip. The unit weight of the soil was assumed as $\gamma = 18$ kN/m^3. A comprehensive ground investigation program comprising approximately 70 CPT soundings was carried out across the site per Fig. 1. The average spacing between CPTs is 40–80 m. The mean q_c within the upper 3 m varies between approximately 3 and 9 MPa across the investigated area, reflecting moderate-to-significant lateral variability.

The spatial distribution of qc was modelled using SGS conditioned on all available (~70) CPT data. The simulation was performed on a three-dimensional grid with 10 × 10 × 0.1 m block dimensions. 100 conditional realizations (i.e., plausible spatial fields of q_c) were generated from conditioning data of the 24 CPTs nearest to each grid. The experimental variogram of the transformed q_c was fitted with a nested model comprising two spherical horizontal structures and a Gaussian vertical structure (Table 1) to characterize its spatial variability. The anisotropic model captures the different scales of spatial correlation in the two principal horizontal directions, with ranges of 150.5 m

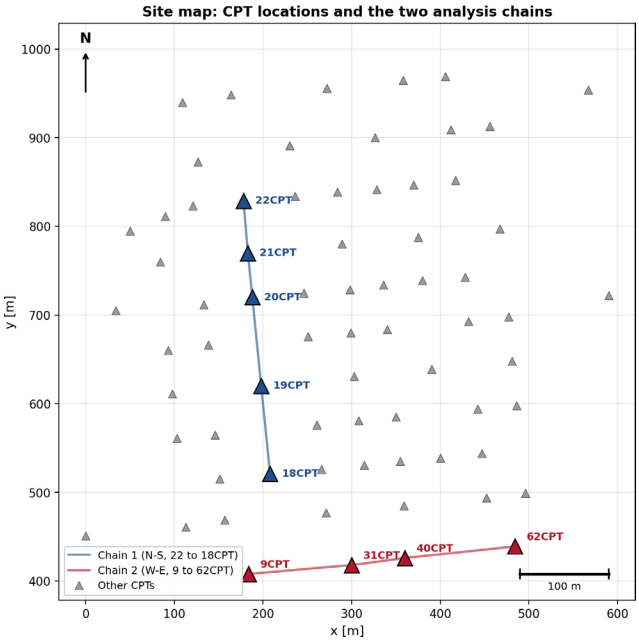

Fig. 1 Site plan showing the locations of approximately 70 CPT soundings (gray triangles), Chain 1 (22-21-20-19-18CPT, north-south, blue), and Chain 2 (9-31-40-62CPT, west-east, red)

Table 1 Variogram parameters for the SGS model of q_c

Structure	Model	Nugget	Sill	Range (m)
Horiz. 1 (az. 358°)	Spherical	0.003	0.23	150.5
Horiz. 2 (az. 88°)	Spherical	0.003	0.23	110.8
Vertical	Gaussian	0.003	0.23	1.05

at an azimuth of 358° and 110.8 m at an azimuth of 88°, while the much shorter vertical range of 1.05 m reflects the finely layered nature of the alluvial deposits. A nugget effect of 0.003 was included in the model to account for short-scale measurement variability and microscale heterogeneity below the resolution of the simulation grid. This nugget value was determined during the automated variogram fitting procedure and is shared across all three directional structures; it represents the spatially uncorrelated component of the variance that persists at lag distances shorter than the smallest voxel dimension (0.1 m vertically, 10 m horizontally).

Two Chains of CPTs were selected to demonstrate the proposed approach for the reliability analysis of pile tensile resistance. The first Chain consists of five real CPTs (22CPT, 21CPT, 20CPT, 19CPT, 18CPT) arranged along an approximately straight, 309 m long north-south line in a geologically uniform zone of the site, with 59, 50, 100 and 99 m spacing between respective CPT locations. Along this line, 27 additional virtual CPT points were placed at 10 m intervals between the real soundings, yielding 32 analysis locations in total. The second Chain comprises four real CPTs (9CPT, 31CPT, 40CPT, 62CPT) along a 302 m long west-east line in a markedly variable geological zone, with inter-CPT spacings of 116, 60 and 125 m, supplemented by 27 virtual CPT points to give 31 analysis locations in total. The two regions were selected because the constituent CPTs lie approximately in a straight line (the maximum perpendicular deviation from the best-fit line is under 1.5 m in both cases), and other CPTs nearest to the Chains lie at least 25–30 m away, so the conditioning effect of off-Chain CPTs on the simulated variance is negligible. At each analysis point (virtual and real CPT locations), a simulated CPT profile was extracted from each of the 100 realizations, providing $q_c(z)$ at 0.1 m depth intervals. These virtual profiles serve as input to the pile capacity calculations.

The pile uplift resistance, R_t, was computed for a driven HEA 160 steel pile with 3 m embedment length, typical in solar panel foundations. The pile has a flange width $b = 160$ mm, section depth $h = 152$ mm, and effective perimeter $P = 2 \times (b + h) = 624$ mm (circumscribed rectangle, assuming soil plugging between flanges). The equivalent radius is $R^* = \sqrt{(b \cdot h/\pi)} = 88$ mm and the equivalent diameter $D^* = 176$ mm. Three direct CPT-based methods were applied to compute the unit shaft friction in tension, q_s, at 0.1 m intervals along the pile shaft. These three methods were originally developed and validated primarily for deeper driven piles (embedment depths of 10–40 m) and larger load magnitudes [10, 12, 13], but have been shown to be applicable to shorter pile segments provided that the shaft friction is integrated over the actual embedded length and that the lower-bound friction fatigue limit ($h/R^* \geq 8$ in ICP-05) is respected. The resulting pile capacities in this study are in the range of 30–80 kN, which is lower than the typical calibration range of these methods; the method uncertainty is therefore larger than for deeper piles and is a key motivation for including three independent estimation approaches and for recommending site-specific pull-out test calibration. All three methods take the cone tip resistance, q_c, as the primary input and use the Robertson I_c index to select the soil-type-dependent coefficients. This ensures that the soil classification varies naturally between SGS realizations and is internally consistent with the q_c profile from which it is derived.

First, the LCPC method of Bustamante and Gianeselli [12] adopts a purely empirical formula, in which the unit shaft friction is obtained by dividing q_c by a soil- and pile-type-dependent coefficient α and capping the result at a limiting value $q_{s,\max}$:

$$q_s = \min\left[\frac{q_c}{\alpha}; q_{s,\max}\right] \cdot \eta.$$

For driven steel piles in sand, the LCPC coefficients depend on the magnitude of the cone tip resistance: for q_c < 5 MPa, α = 120, and $q_{s,\max}$ = 35 kPa; for 5 MPa ≤ q_c < 12 MPa, α = 200, and $q_{s,\max}$ = 80 kPa; and for $q_c \geq$ 12 MPa, α = 200, and $q_{s,\max}$ = 120 kPa. In finer-grained soils (I_c greater than 2.60), α = 60 and $q_{s,\max}$ = 15 kPa are adopted. The factor η_t = 0.70 converts the compressive shaft friction to its tensile counterpart.

Second, the NF P 94-262 standard [13] by the AFNOR adopts a nonlinear formulation for the unit shaft friction. Instead of a simple linear scaling of q_c, the method computes a soil-dependent function:

$$f_{sol} = \left(a \cdot q_c + b\right) \cdot \left(1 - e^{-c \cdot q_c}\right),$$

where the coefficients a, b and c depend on the soil type determined *via* the Robertson I_c classification. The unit shaft friction is then calculated by the formula:

$$q_s = \min\left(\alpha_s \cdot f_{sol} \cdot q_c ; q_{s,\max}\right) \cdot \eta_t,$$

where η_t = 0.70 is the tension reduction factor. For clean sand (I_c < 2.05): a = 0.0012, b = 0.1, and c = 0.15 with α_{ps} = 0.70 and $q_{s,\max}$ = 130 kPa; for sand-mix soils (2.05 < I_c < 2.60): a = 0.0015, b = 0.1, and c = 0.25 with α_{ps} = 0.65 and $q_{s,\max}$ = 90 kPa; for cohesive soils (I_c > 2.60): a = 0.0018, b = 0.1, and c = 0.40 with α_{ps} = 0.55 and $q_{s,\max}$ = 90 kPa.

Third, the ICP-05 method [10] departs from the empirical α-based framework and adopts a mechanistic effective stress formulation instead. The unit shaft friction is computed as the product of the post-installation radial effective stress σ'_{rc} and the tangent of the constant-volume interface friction angle δ_{cv}, with an additional factor accounting for the difference between compression and tension:

$$q_s = \eta \cdot \left(\sigma'_{rc} + \Delta\sigma'_{rd}\right) \cdot \tan\delta_{cv},$$

where, for steel piles in sand, δ_{cv} = 28°, and η = 0.75 (a smaller reduction adopted by ICP-05 relative to LCPC), while σ'_{rc} for the for ICP-05 method is given by:

$$\sigma'_{rc} = 0.029 \cdot q_c \cdot \left(\frac{\sigma'_{v0}}{p_a}\right)^{0.13} \cdot \left(\frac{h}{R^*}\right)^{-0.38},$$

where σ'_{v0} is the vertical effective stress at the given depth, p_a = 100 kPa is the atmospheric reference pressure, h is the distance from the pile tip to the given depth (so that h decreases with depth toward the tip), and R^* is the equivalent pile radius for non-circular sections.

$\Delta\sigma'_{rd}$ is the dilation-induced radial stress increment computed from the cylindrical cavity expansion solution as:

$$\Delta\sigma'_{rd} = 4 \cdot G \cdot \frac{\Delta r}{D^*},$$

where G is the shear modulus of the surrounding soil estimated from the cone tip resistance *via*:

$$G = 185 \frac{q_c}{\left(q_{c1N}\right)^{0.7}};\ q_{c1N} = \frac{q_c / p_a}{\sqrt{\sigma'_{v0} / p_a}},$$

where Δr = 0.02 mm is the typical interface dilation for clean steel-sand contacts under pull-out [10], and $D^* = 2R^*$ is the equivalent pile diameter for the non-circular HEA 160 cross-section. The $\Delta\sigma'_{rd}$ term applies only to granular soils ($I_c \leq 2.60$); in cohesive soils the ICP-05 method reverts to the original total-stress formulation.

In the equation for σ'_{rc}, the $\left(\sigma'_{v0}/p_a\right)^{0.13}$ term introduces a mild dependence on overburden pressure, while the $(h/R^*)-0.38$ term captures the well-documented friction fatigue effect, by which the radial stress at any given depth degrades as the pile is driven further past that depth. A lower bound of h/R^* = 8 is imposed according to the ICP-05 method to prevent an unrealistic over-prediction of the unit friction near the pile tip, where the formula may diverge.

The total uplift resistance, R_t, along the 3 m solar panel pile was obtained by integrating the unit shaft friction over its embedded length, considering P = 0.624 m effective perimeter of the HEA 160 section (including soil plug between the flanges). Because each SGS realization yields a complete q_c profile for each realization, this integration is performed independently for all 100 realizations, producing an ensemble of 100 R_t values per analysis point, per capacity method. The mean μ_R, standard deviation σ_R, and 5th and 95th percentiles of this ensemble characterize the predictive uncertainty of the uplift resistance at any location.

The reliability index β was evaluated using two methods of increasing rigor. The First-Order Second-Moment (FOSM) approach and the First-Order Reliability Method (FORM). First, based on the limit state function $G = R_t - S$, where S is the applied uplift load, the FOSM reliability index was computed as:

$$\beta_{\text{FOSM}} = \frac{\mu_R - \mu_S}{\sqrt{\sigma_R^2 + \sigma_S^2}},$$

where μ_R and σ_R are the mean and standard deviation of the R_t ensemble. The FOSM approach is consistent with a normal-tail approximation of both the resistance and the load.

Second, the First-Order Reliability Method (FORM) was implemented based on the same limit state function with both R_t and S modelled as lognormal random variables. As the limit state in the log-space is linear for

lognormally distributed R_t and S, the FORM reliability index has the closed-form solution:

$$\beta_{\text{FORM}} = \frac{\lambda_R - \lambda_S}{\sqrt{\zeta_R^2 + \zeta_S^2}},$$

where $\lambda = \ln(\mu) - 0.5 \cdot \zeta^2$ and are the parameters of the underlying normal distribution of $\ln(R_t)$ and $\ln(S)$. The log-normally distributed uplift load has a mean of $\mu_S = 20$ kN, and a coefficient of variation $\text{COV}_S = 0.20$, giving $\sigma_S = 4$ kN. This corresponds to the wind-induced uplift force on a single pile under a fixed-tilt photovoltaic panel of moderate dimensions in flat terrain [2, 4]. The COV of 0.20 reflects the combined uncertainty of wind speed, panel configuration, and load model, consistent with the variability reported for wind loads on structures in EN 1990 standard [21] and with values adopted in comparable reliability studies of solar farm foundations [2]. The load's equivalent characteristic value under EN 1991-1-4 standard [9] quantile conventions is $S_k = \mu_S \times 1.1 = 22$ kN.

4 Results

As a result of the sequential Gaussian simulation (SGS) detailed previously, the expected (mean) q_c values were established for the entire investigated area depicted in Fig. 1, alongside their exact simulated values for each conditional realization. Consequently, the q_c profile corresponding to each realization could be extracted at any arbitrary location within the model domain, allowing for the robust determination of its statistical distribution. An example realization along Chain 1 is depicted in Fig. 2, while Fig. 3 illustrates the ensemble of realizations near an actual CPT sounding (19CPT), and one with at the midpoint between 18CPT and 19CPT. It is obvious from the figures that the simulated profiles tightly cluster around the measured q_c at the point near 19CPT, whereas further away from this conditioning point the increased kriging variance produces a noticeably wider spread of realizations.

The statistical distributions of the pile uplift resistance calculated at these two points are illustrated in Fig. 4. Comparing the histogram of the well-conditioned location (close to 19CPT) with that of the midpoint between

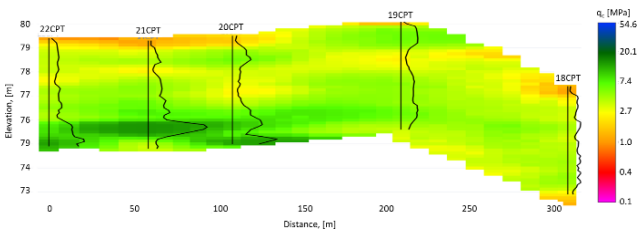

Fig. 2 q_c profile obtained by SGS along Chain 1

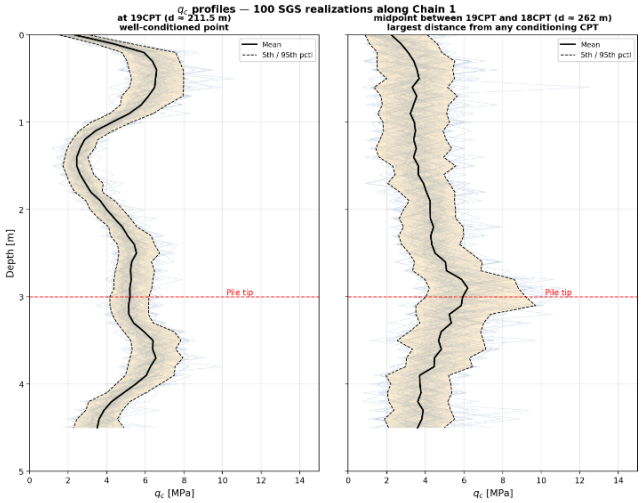

Fig. 3 q_c profiles at 19 CPT and at the midpoint between 18CPT and 19CPT

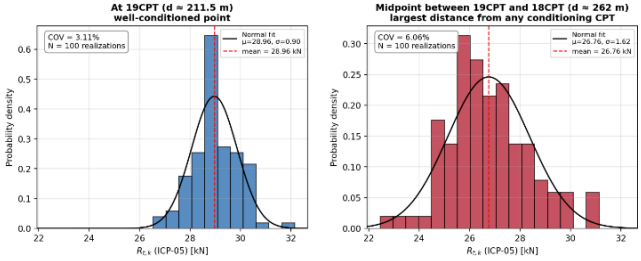

Fig. 4 Histograms of bearing capacities

19CP and 18CPT, the increasing uncertainty with increasing distance from existing CPT soundings is pronounced.

Using the nodal data, the Chain-based analysis is conducted to produce two complete uncertainty profiles. One along Chain 1 (N-S direction, 32 analysis points) and one along Chain 2 (W-E direction, 31 analysis points), per Fig. 1. The mean and variability of the pile uplift resistance estimates given by the three CPT-based formulas, as well as the corresponding FOSM and FORM reliability indices are generated along each Chain. The complete numerical results are provided as supplementary spreadsheets, while the most important findings are summarized below.

4.1 Chain 1: N-S Direction (Homogeneous Soil Zone)

The three CPT-based capacity methods produce clearly different mean resistance levels along Chain 1, as shown by Fig. 5. The AFNOR method, with its nonlinear f_{sol} formulation, yields the highest mean resistance values (μ_R = 45–54 kN), followed by the LCPC method (37–42 kN) and the ICP-05 method (35–44 kN). Although the mean values differ, the spatial pattern of the resistance is remarkably consistent across the three methods. All three exhibit the same wavy variation along the Chain, with local maxima at the positions of existing CPT sounding and

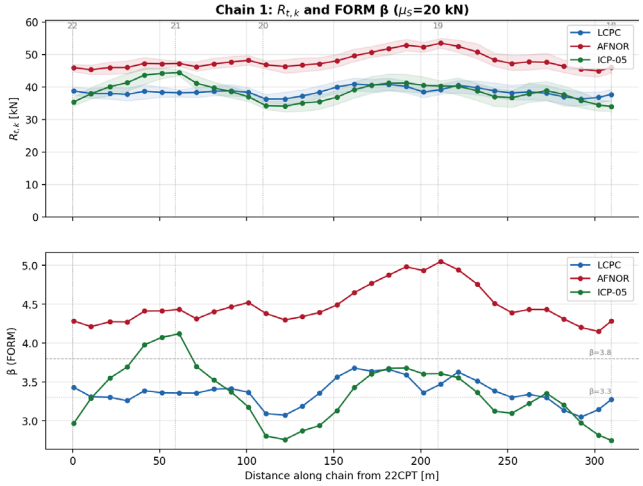

Fig. 5 Chain 1: mean uplift resistance with P5-P95 confidence bands (top), and FORM reliability index for μ_s = 20 kN (bottom), for the three CPT-based methods

minima at their midpoints. The LCPC and ICP-05 methods produce nearly identical mean resistance values along the Chain (within approximately 10%), while the AFNOR method gives systematically higher values by approximately 25–40%. Importantly, the COV of R_t is very similar across all three methods at any given location, per Fig. 6. This consistency indicates that the relative uncertainty in the resistance is governed by the underlying q_c uncertainty rather than the structure of the empirical uplift capacity formulas. The wavy pattern of COV along the Chains (Figs. 6 to 8) are reproduced consistently by all three methods, therefore, the choice of method will only affect the value of the reliability index, not its spatial pattern.

The FORM reliability index, β_{FORM}, (Fig. 5) along Chain 1 varies between 2.75 (at the 18CPT endpoint) and 4.12 (at 21CPT) for the ICP-05 method, between 3.07 and 3.68 for LCPC, and between 4.21 and 5.05 for NF P 94-262 standard [13]. Using the ICP-05 and LCPC methods, the target reliability (β_{FORM} = 3.3) is exceeded only at the well-conditioned Chain points near 21CPT and 19CPT, while at the midpoints and Chain endpoints β_{FORM} falls below the target. With the NF P 94-262 standard [13] method, β_{FORM}

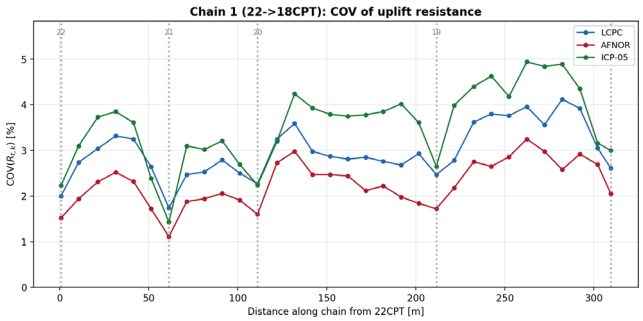

Fig. 6 Chain 1 (22CPT → 18CPT, N → S): COV of the uplift resistance for the three CPT-based methods

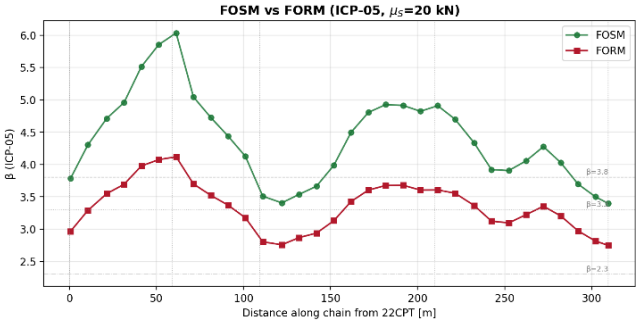

Fig. 7 Chain 1: FOSM and FORM reliability index along the Chain. Horizontal lines indicate target reliability levels β = 2.3, 3.3 and 3.8 from EN 1990 standard [21]

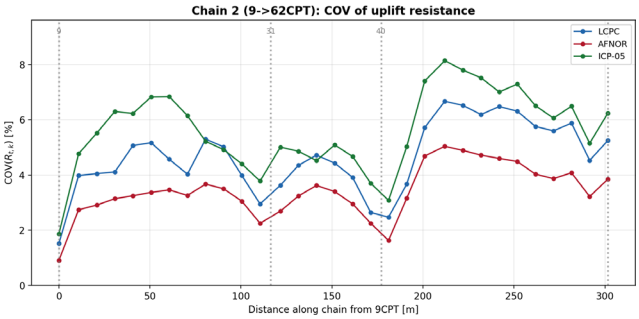

Fig. 8 Chain 2 (9CPT → 62CPT, W → E): COV of the uplift resistance for the three CPT-based methods

exceeds 3.8 at every point along Chain 1. As shown in Fig. 7, the FOSM reliability index is consistently higher than the FORM value by approximately 0.4–1.0 units, reflecting the effect of the lognormal tail approximation.

Table 2 summarizes the numerical results at selected points along Chain 1, highlighting the wavey, rising-then-dipping pattern of the COV and reliability index corresponding to positions far from- and near to existing CPT sounding locations.

4.2 Chain 2: W-E Direction (Variable Soil Zone)

Chain 2 traverses a much more variable soil environment. The depth-averaged q_c ranges from 3.16 MPa near

Table 2 Selected results along Chain 1 (ICP-05, μ_s = 20 kN)

d (m)	Position	$q_{c,avg}$ (MPa)	μ_R (kN)	COV (%)	β_{FOSM}	β_{FORM}
0.7	22CPT	3.69	35.43	2.23	3.79	2.97
31.4	mid 22–21	4.13	41.35	3.85	4.96	3.69
61.3	21CPT	4.41	44.44	1.43	6.03	4.12
91.2	mid 21–20	4.06	38.59	3.21	4.44	3.37
111.1	20CPT	3.76	34.30	2.24	3.51	2.80
151.8	mid 20–19	3.97	36.89	3.79	3.99	3.13
211.5	19CPT	4.57	40.32	2.65	4.91	3.61
262.3	mid 19–18	3.97	37.91	4.94	4.06	3.22
309.5	18CPT	3.56	34.03	3.00	3.40	2.75

the center of the Chain (around d = 100 m from 9CPT) to 9.27 MPa near the 270 m mark, almost a threefold difference. As a result, the mean uplift resistance (per ICP-05) varies from R_t = 32.1 kN at the weakest point to 75.2 kN at the strongest; a factor of 2.3 that directly reflects the variability of soil strength rather than the conditioning geometry (i.e., the spatial configuration of the existing CPT sounding points used in the kriging system). The COV pattern (Fig. 8) retains the wavy structure observed along Chain 1, but its amplitude is higher. The local minima at the existing CPT positions reaches 1.9–3.8%, while the maxima half-way between existing CPTs rises to 7–8%, where the inter-CPT spacings are the largest. The mean resistance and FORM reliability index profiles along Chain 2 are shown in Fig. 9, and the FOSM *vs.* FORM comparison is given in Fig. 10. The FORM reliability index along Chain 2 for R_t, calculated *via* the ICP-05 method, ranges from 2.42 in the weak soil zone (around d = 100 m from 9CPT, where q_c is lowest) to 6.48 in the eastern strong soil zone (around d = 270 m, where q_c reaches its maximum). The contrast with Chain 1 is striking, along Chain 1 the

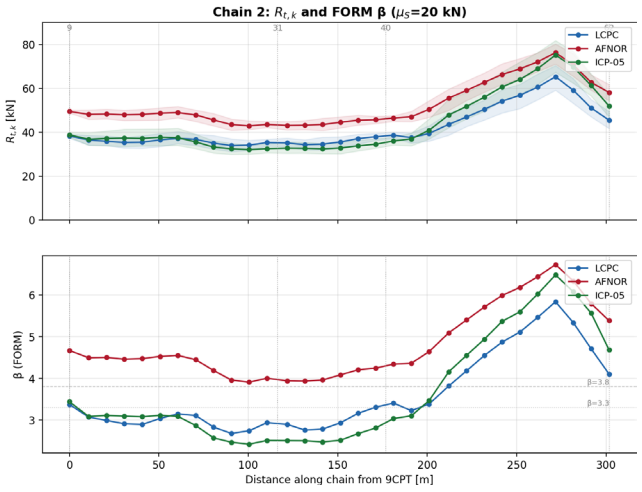

Fig. 9 Chain 2: mean uplift resistance with P5–P95 confidence bands (top), and FORM reliability index for μ_s = 20 kN (bottom), for the three CPT-based methods

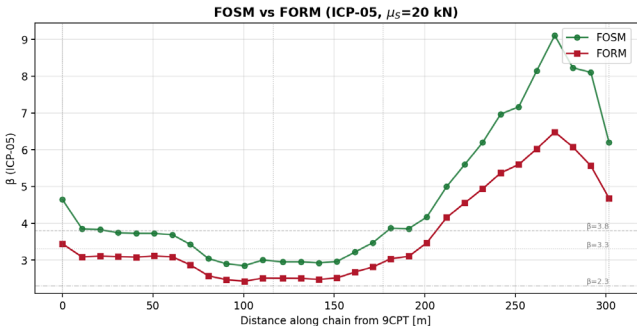

Fig. 10 Chain 2: FOSM and FORM reliability index along the Chain (ICP-05 method, μ_s = 20 kN)

β variation is approximately 1.4 units and is driven almost entirely by the conditioning geometry, while along Chain 2 it spans more than 4 units and is dominated by the strong spatial variation in soil strength.

The western half of Chain 2 (0–200 m) remains the most critical part of the site. With the ICP-05 method, β_{FORM} stays below 3.3 over a contiguous stretch from approximately 70 to 170 m, reaching a minimum of 2.42 near the center of the Chain where the soil is the weakest. The LCPC method gives marginally higher values (β_{FORM} = 2.68–5.84) across the weak zone. The NF P 94-262 standard [13] method, however, maintains β_{FORM} above 3.9 even in the weak zone of Chain 2, with a minimum of 3.91. In the eastern half (200–290 m), all three methods produce β_{FORM} well above 3.3, with ICP-05 reaching 6.48 and NF P 94-262 standard [13] reaching 6.73 at the point with the strongest soil, near 270 m. The contrast with Chain 1 remains striking, along Chain 1 the β_{FORM} variation is approximately 1.4 units (ICP-05), while along Chain 2 it spans more than 4 units, confirming that the geological variability dominates the reliability index of uplift capacity in the heterogeneous zone.

Table 3 summarizes the numerical results at selected points along Chain 2, illustrating the dominant role of the spatial variability of soil strength.

The FORM reliability index is consistently lower than the FOSM value across all analysis points along Chain 2. The difference for the ICP-05 method ($\Delta\beta$) is approximately 0.3–1.0.

The systematic discrepancy between the FOSM and FORM β values are due to the difference in the assumed distribution of the random variables between the two methods. FOSM assumes normal, while FORM uses lognormal distribution. The errors introduced by assuming a normal distribution originates from two related sources. First, the underlying cone tip resistance, q_c, does not follow a normal distribution but is much closer to a lognormal distribution.

Table 3 Selected results along Chain 2 (ICP-05, μ_s = 20 kN)

d (m)	Position	$q_{c,avg}$ (MPa)	μ_R (kN)	COV (%)	β_{FOSM}	β_{FORM}
0.0	9CPT	4.02	38.89	1.87	4.64	3.44
50.7	midpoint 9–31	3.88	37.73	6.83	3.73	3.11
100.5	midpoint 9–31	3.16	32.09	4.40	2.85	2.42
110.5	31CPT	3.30	32.55	3.78	3.00	2.51
141.5	midpoint 31–40	3.28	32.48	4.52	2.92	2.48
171.3	40CPT	3.62	34.58	3.70	3.47	2.81
241.9	midpoint 40–62	7.34	60.74	7.01	6.97	5.37
271.7	midpoint 40–62	9.27	75.24	6.06	9.11	6.48
301.6	62CPT	5.82	51.94	6.24	6.20	4.68

Second, the Chain of transformations from, q_c, to the uplift resistance, R_r, is non-linear throughout all the three CPT-based calculation methods, therefore, even if q_c were normally distributed, the resulting R_t would not be.

5 Discussion

The combined results from the two Chains support a key conclusion on the reliability of CPT-designed piles: the spatial variation of the reliability index along a CPT investigation grid arises from two largely independent contributions. Namely the kriging variance of the simulated soil profile, which depends on the geometric distance to the nearest conditioning CPTs, and the actual change in the local soil strength, which depends on the geological variability of the deposit. The Chain-based sampling strategy makes the two contributions directly visible. Along Chain 1, where the geology is uniform, the variation of β is dominated by the wavy conditioning pattern (β is inversely proportional with relative distance from the closest CPT location), whereas along Chain 2, where the geology varies markedly, the same wavy pattern is overshadowed by a much stronger trend driven by the change in soil strength. In a geologically homogeneous setting such as Chain 1, the most direct way to improve the local reliability is to densify the CPT investigation grid, consistent with the spirit of the Eurocode 7 [6] correlation factors. Conversely, in a geologically variable setting such as Chain 2, the rational design strategy is to delineate the geologically distinct zones and treat each as a separate design unit, also fully aligned with the Eurocode 7 [6] framework.

The Eurocode 7 [6] partial factor approach uses correlation factors that depend solely on the number of profiles and do not account for the spatial arrangement, local CPT density, or geological variability. Along Chain 1, the maximum permissible characteristic uplift force on solar panel piles, $S_{k,\max}$, for a target $\beta_{\mathrm{FORM}} = 3.3$, the permissible characteristic uplift force $S_{k,\max}$ (range and spread) by method is summarised below. Chain 1 (uniform zone): ICP-05: 19.7–25.9 kN (31% spread); LCPC: 20.9–23.8 kN (14% spread); NF P 94-262 standard [13]: 26.1–31.2 kN (20% spread). Chain 2 (variable zone): ICP-05: 18.4–42.6 kN; LCPC: 19.4–37.1 kN; NF P 94-262 standard [13]: 24.9–44.0 kN. The three capacity methods differ by up to 40% in predicted mean uplift resistance but yield identical spatial COV patterns. The NF P 94-262 standard [13] method produces the highest values and achieves β_{FORM} above 3.8 across the entire site, while LCPC and ICP-05 fall below $\beta_{\mathrm{FORM}} = 3.3$ at distant points from existing CPT sounding locations and in weak soil zones. This model uncertainty can be substantially reduced by performing a small number of static pile pull-out tests at the site, allowing the practitioner to identify the most accurate method and utilize it for pile design across the entire solar farm. A pragmatic intermediate solution is to derive site-specific correction factors akin to the standard EC7 correlation factors, which represents a promising direction for future development.

Several limitations warrant further investigation. The analysis considers a single pile type (HEA 160) at a single embedment depth (L = 3.0 m). The load COV is fixed at 0.20. The Chain-based sampling assumes negligible conditioning effect of off-Chain CPTs, which was verified at 25–30 m distances in this study, but may not apply for denser SGS grids. Despite these limitations, the framework provides a transparent basis for separating the geometric and geological contributions to the reliability of solar panel pile uplift capacity and can be extended to other pile types and multi-site optimization studies.

6 Conclusions

The reliability of CPT-designed driven piles supporting solar panels is governed by two distinct contributions. A geometric component based on the SGS conditioning, showing wavy COV profile along a chain of CPT tests with kriging-variance-driven minima at CPT positions and maxima at their midpoints, and a geological component from the actual soil strength variability. The proposed Chain-based sampling strategy separates these cleanly. Along the analyzed Chain 1, where the soil was uniform, the wavy pattern reflects almost exclusively the conditioning geometry, while along Chain 2, where the soil was highly variable, it is overshadowed by a much stronger geological trend following the change in soil strength.

For design practice, densifying the CPT grid is effective in zones with uniform soils, while delineating geotechnical units is the recommended priority in zones with highly variable soils. In this study, the partial factor approach with uniform correlation factors produced reliability that varies by 31% along the uniform Chain 1 and by more than a factor of two along the variable Chain 2.

The model uncertainty stemming from the choice of pile uplift capacity estimation method was shown to be comparable to the spatial uncertainty in within a uniform soil zone. The three methods differ by up to 40% in mean resistance but produce identical spatial COV patterns. This model uncertainty can be substantially reduced by performing a small number of static pull-out tests at a project site, allowing the selection of the most accurate method in an Eurocode-compliant manner.

The combination of Chain-based SGS analysis with site-specific load test calibration opens the door to genuine reliability-based design of solar power foundations, in which pile embedded lengths can be adjusted locally to adhere to a prescribed target reliability index. The follow-up work will extend the framework to a multi-site database with the objective of optimizing the trade-off between investigation density, pile length, and target reliability. Beyond solar farm foundations, the Chain-based SGS framework can be applied to any geotechnical design problem where linear infrastructure (roads, pipelines, embankments) intersects a spatially variable deposit and where the distance from ground investigation points to the design cross-section governs uncertainty, including slope stability assessments, pavement subgrade design, and buried pipeline routing.

Acknowledgement

Project no. [2023-1.1.1-PIACI_FÓKUSZ-2024-00048] has been implemented with the support provided by the Ministry of Culture and Innovation of Hungary from the National Research, Development and Innovation Fund, financed under the [2023-1.1.1-PIACI_FÓKUSZ] funding scheme.

This research was supported under the Shenzhen Overseas High-Caliber Personnel Peacock Plan, 827-000947.

References

[1] IFC "Utility-Scale Solar Photovoltaic Power Plants: A Project Developer's Guide", [pdf] International Finance Corporation, Washington, DC, USA, 2015. Available at: https://ppp.worldbank.org/sites/default/files/2022-03/IFC_Solar_Report_Web__08_05.pdf [Accessed: 01 May 2026]

[2] Kelly, R., Huang, J., Poulos, H., Stewart, M. G. "Geotechnical and Structural stochastic analysis of piled solar farm foundations", Computers and Geotechnics, 132, 103988, 2021. https://doi.org/10.1016/j.compgeo.2020.103988

[3] Decker, J. B., Rollins, K. M., Ellsworth, J. C. "Corrosion Rate Evaluation and Prediction for Piles Based on Long-Term Field Performance", Journal of Geotechnical and Geoenvironmental Engineering, 134(3), pp. 341–351, 2008. https://doi.org/10.1061/(ASCE)1090-0241(2008)134:3(341)

[4] Fleming, K., Weltman, A., Randolph, M., Elson, K. "Piling Engineering", CRC Press, 2008. ISBN 9780429181177 https://doi.org/10.1201/b22272

[5] Baecher, G. B., Christian, J. T. "Reliability and Statistics in Geotechnical Engineering", John Wiley & Sons Ltd, 2003. ISBN 0-471-49833-5 [online] Available at: https://download.e-bookshelf.de/download/0000/5803/45/L-G-0000580345-0015292792.pdf [Accessed: 01 May 2026]

[6] CEN "EN 1997-1 Eurocode 7: Geotechnical design – Part 1: General rules", European Committee for Standardization, Brussels, Belgium, 2004. [online] Available at: https://www.ngm2016.com/uploads/2/1/7/9/21790806/eurocode_7_-_geotechnical_designen.1997.1.2004.pdf [Accessed: 01 May 2026]

[7] Bond, A., Harris, A. "Decoding Eurocode 7", Taylor & Francis, 2008. ISBN 0-415-40948-9

[8] Barbón, A., Bayón-Cueli, C., Bayón, L., Carreira-Fontao, V. "A methodology for an optimal design of ground-mounted photovoltaic power plants", Applied Energy, 314, 118881, 2022. https://doi.org/10.1016/j.apenergy.2022.118881

[9] CEN "EN 1991-1-4 Eurocode 1: Actions on structures – Part 1-4: General actions – Wind actions", European Committee for Standardization, Brussels, Belgium, 2005. [online] Available at: https://www.phd.eng.br/wp-content/uploads/2015/12/en.1991.1.4.2005.pdf [Accessed: 01 May 2026]

[10] Jardine, R., Chow, F., Overy, R., Standing, J. "ICP design methods for driven piles in sands and clays", Emerald Publishing Limited, 2005. ISBN 978-0-7277-3272-9 https://doi.org/10.1680/idmfdpisac.32729

[11] Frank, R., Bauduin, C., Driscoll, R., Kavvadas, M., Krebs Ovesen, N., Orr, T., Schuppener, B. "Designers' Guide to EN 1997-1: Eurocode 7: Geotechnical design – General rules", Thomas Telford, 2005. ISBN 978-0-7277-3154-8 [online] Available at: https://bouassidageotechnics.wordpress.com/wp-content/uploads/2022/03/designers-guide-to-eurocode-7-geotechnical-design-en-1997.pdf [Accessed: 01 May 2026]

[12] Bustamante, M., Gianeselli, L. "Pile bearing capacity prediction by means of static penetrometer CPT", In: Proceedings of the 2nd European Symposium on Penetration Testing, Amsterdam, Netherlands, 1982, pp. 493–500. ISBN 978-90-6191-252-1

[13] AFNOR "NF P 94-262 Justification des ouvrages géotechniques – Fondations profondes" (NF P 94-262 Justification of geotechnical work – Deep foundations), AFNOR, Paris, France, 2012. (in French)

[14] Robertson, P. K. "Interpretation of cone penetration tests — a unified approach", Canadian Geotechnical Journal, 46(11), pp. 1337–1355, 2009. https://doi.org/10.1139/T09-065

[15] Orr, T. L. L., Bergdahl, U., Frank, R., Scarpelli, G., Simpson, B. "Evaluation of Eurocode 7: Geotechnical design", In: Proceedings of the International Workshop on Evaluation of Eurocode 7, Dublin, Ireland, 2005, pp. 1–10. ISBN 978-1-607500-31-5

[16] Chemali, B., Tiliouine, B. "Probabilistic Analysis of Shallow Foundations on c-φ Soils Using 2nd Order Response Surface Methods", Periodica Polytechnica Civil Engineering, 67(2), pp. 485–494, 2023. https://doi.org/10.3311/PPci.17917

[17] Cai, Y., Bransby, F., Gaudin, C., Uzielli, M. "A framework for the design of vertically loaded piles in spatially variable soil", Computers and Geotechnics, 134, 104140, 2021. https://doi.org/10.1016/j.compgeo.2021.104140

[18] Cai, Y., Bransby, F., Gaudin, C., O'Neill, M., Uzielli, M. A "CPT-Based Design Framework for Uplifted Open-Ended Piles Installed in Spatially Variable Sandy Soils. II: Implications to Site Investigation and Pile Design for Offshore Wind Farms", Journal of Geotechnical and Geoenvironmental Engineering, 149(11), 04023098, 2023. https://doi.org/10.1061/JGGEFK.GTENG-11392

[19] Phoon, K.-K., Kulhawy, F. H. "Characterization of geotechnical variability", Canadian Geotechnical Journal, 36(4), pp. 612–624, 1999. https://doi.org/10.1139/t99-038

[20] Phoon, K.-K., Kulhawy, F. H. "Evaluation of geotechnical property variability", Canadian Geotechnical Journal, 36(4), pp. 625–639, 1999. https://doi.org/10.1139/t99-039

[21] CEN "EN 1990 Eurocode – Basis of structural design", European Committee for Standardization, Brussels, Belgium, 2002. [online] Available at: https://www.phd.eng.br/wp-content/uploads/2015/12/en.1990.2002.pdf [Accessed: 01 May 2026]

[22] Vanmarcke, E. "Random Fields: Analysis and Synthesis", World Scientific, 2010. ISBN 9789812563538

[23] Deutsch, C. V., Journel, A. G. "GSLIB: Geostatistical Software Library and User's Guide", Oxford University Press, 1997. ISBN 0195100158

[24] Chilès, J.-P., Delfiner, P. "Geostatistics: Modeling Spatial Uncertainty", John Wiley & Sons Ltd, 2012. ISBN 978-0-470-18315-1

[25] Journel, A. G., Huijbregts, C. J. "Mining Geostatistics", Academic Press Inc., 1978. ISBN 0-12-391050-1